REFLECTOMETRY: ANALYTICAL AND NUMERICAL MODELLING OF PHASE VARIATIONS WITH LARGE AMPLITUDE DENSITY FLUCTUATIONS

I. Boucher, C. Fanack, S. Hacquin, S. Heuraux, G. Leclert, F. Clairet* and X.L. Zou*

LPMI, Unité CNRS 7040, Université Henri Poincaré Nancy,
54506 Vandoeuvre Cedex, France
**DRFC, CE Cadarache, CEA, 13108 St Paul-lez-Durance Cedex, France*

1. Introduction and basic equations

Reflectometry is widely used in fusion plasma experiments. Density fluctuations can produce difficulties in interpreting phase data, either because of the breakdown of the Born approximation, or the distortion of the cutoff layer due to poloidal fluctuation wave-numbers [1,2,3,4].

We present here results of one- and two-dimensional full-wave codes that solve the Helmholtz equation, for quasi-monochromatic perturbations, i.e. a sine wave with a Gaussian or square envelope. The problem of nonlinear phase response is treated in the first part. In order to understand the underlying physics we use a one-dimensional full-wave code for two cases of large amplitude fluctuations, which either resonantly backscatter the incident wave, or are located close to the cutoff layer. For the resonant fluctuations, we describe an analytical model that is in a good agreement with the numerical results. For the non-resonant case, an empirical law is found in terms of the system parameters. In the second part, the influence of azimuthal perturbations is studied with a full-wave two-dimensional code.

The steady-state ordinary wave propagation obeys the Helmholtz equation:

$$\nabla^2 E + k_0^2 N_0^2(x,y)E = \nabla^2 E + k_0^2\left(1 - \frac{n_0(x,y)}{n_{cr}} - \frac{\delta n(x,y)}{n_0}\right)E = 0 \qquad (1)$$

where $N_0(x,y)$ is the O-mode refractive index, $n_0(x,y)$ the unperturbed density, n_{cr} the critical (cutoff) density for the frequency $\omega = k_0 c$ and $\delta n(x,y)$ the density perturbation which can be described in case of quasi-monochromatic perturbations like :

$$\delta n(x,y) = \delta n_0 \cos[k_x(x - x_f) + k_y(y - y_f)]\, f(x) \qquad (2)$$

with f(x) = $\exp[-(x - x_f)^2 / w_f^2]$ (Gaussian) or f(x) = $\begin{cases} 1 \text{ if } |x - x_f| < w_f \\ 0 \text{ if } |x - x_f| > w_f \end{cases}$ (wave-train)

The x and y coordinates represent the radial and poloidal directions. δn_0 is the perturbation amplitude, (x_f, y_f) its position and w_f its radial half-width. The density gradient is along the x-direction : $n_0(x,y) = n_{cr}(1 + x/L)$. For 1D situations one lets $\nabla \equiv d/dx$ in (1) and $k_y = 0$ in (2).

2. Large amplitude perturbations: 1D model

a. Bragg resonant perturbations

The phase response (i.e. the phase shift versus the perturbation position x_f) has been analyzed in earlier works, at small amplitude [5,6] or slightly beyond the Born approximation [7]. As the amplitude grows, the shape of the phase response becomes both distorted and broader. The fully nonlinear regime is exemplified on Figure 1 for a wave-train perturbation.

The maximum phase shift is now far from the linear Bragg resonance point x_B defined by the Bragg resonant condition $k(x_B) = k_x/2$, and abrupt phase variations occur. This process can be modeled in the following way for a wave-train perturbation. Outside the perturbation, the field is the usual Airy function. Inside the perturbation, the Helmholtz equation can be approximated by a Mathieu equation :

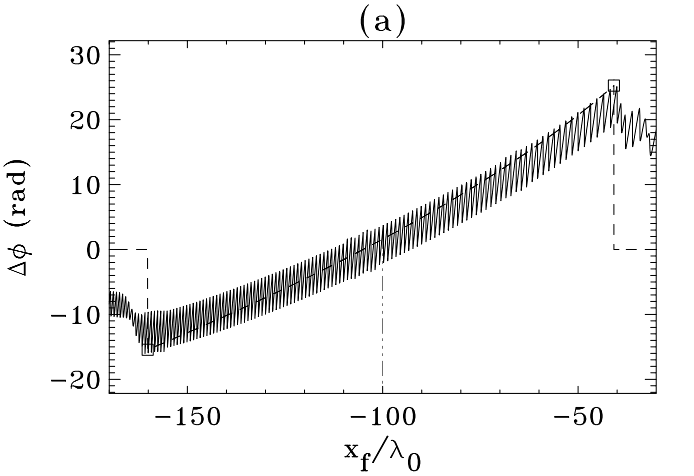

Figure 1. Phase response in the strongly nonlinear regime : Wave-train : $\delta n_0/n_{cr}=0.3$, $L=400\lambda_0$, $w_f=5\lambda_0$, $k_x=1.4k_0$

$$\frac{d^2E}{d\zeta^2} + (p - 2q\cos\zeta)E = 0 \quad ;$$

$$\zeta = \frac{1}{2}k_f(x - x_f);\, p = 4\frac{k_0^2}{k_f^2}\frac{x_f}{L};\, q = 2\frac{k_0^2}{k_f^2}\frac{\delta n_0}{n_{cr}} \tag{4}$$

p and q are the normalized position and amplitude of the perturbation. The Mathieu equation has parameter domains, starting from $p=1,4,9,\ldots,n^2$ at $q=0$, where the solution grows exponentially [8]. The first domain p=1 corresponds to the usual Bragg scattering, see (4). When the perturbation amplitude grows, the unstable domains broaden. To the first order in δn_0, Bragg scattering takes place over the whole region defined by $p=1\pm\Delta q$, that is :

$$\frac{1}{4}\frac{k_f^2}{k_0^2} - \frac{1}{2}\frac{\delta n_0}{n_{cr}} < \frac{x_f}{L} < \frac{1}{4}\frac{k_f^2}{k_0^2} + \frac{1}{2}\frac{\delta n_0}{n_{cr}} \tag{5}$$

In the unstable domains, in accordance with Floquet's [1,2] theorem the solution inside the perturbation can be cast in the form $E = \cos\zeta\exp(\pm\mu\zeta)$. Hence, the field wavelength inside the perturbation becomes constant and equal to twice the perturbation wavelength λ_x. This prediction is well reproduced by the numerical computation, as indicated in Figure 2. From this figure one finds an approximate expression of the mean phase shift in this saturated regime. It is simply the difference, across the perturbation, between the WKB phase shift and the phase shift associated to the constant wavelength $2\lambda_x$. Hence, as long as x_f lies in the unstable region defined by (5), the mean phase shift reads:

$$\Delta\varphi = 4\pi\frac{w_f}{\lambda_x} - 2k_0\int_{x_f - w_f}^{x_f + w_f} N_0(x)dx \tag{6}$$

Hence, the maximum phase shift occurs at the right boundary of the un-stable domain of the Mathieu equation

$$\frac{|x_f|}{L} = \frac{|x_B|}{L} - \frac{1}{2}\frac{\delta n_0}{n_{cr}} \tag{7}$$

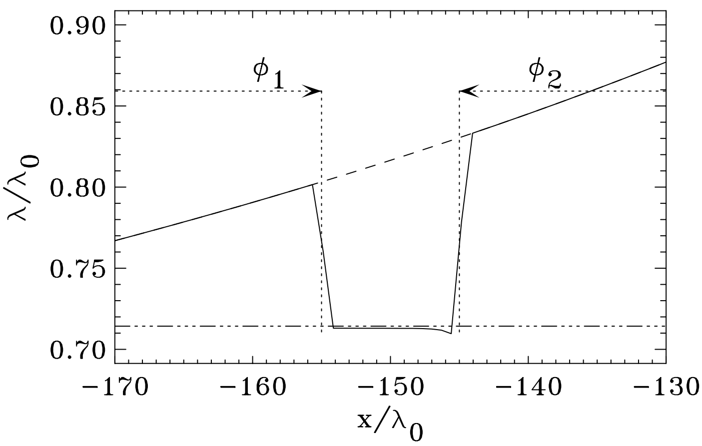

Figure 2. Comparison of the numerical and WKB wavelengths inside the perturbation.

$$\Delta\varphi_{max} = 4\pi \frac{w_f}{\lambda_r} - \frac{8}{3} k_0 L \left[\left(\frac{|x_B|}{L} - \frac{1}{2}\frac{\delta n_0}{n_{cr}} + w_f \right)^{3/2} - \left(\frac{|x_B|}{L} - \frac{1}{2}\frac{\delta n_0}{n_{cr}} - w_f \right)^{3/2} \right] \quad (8)$$

In Figure 1, the squares indicate the analytical predictions (7) and (8). Hence, the agreement is excellent between the numerical computation and the theory.

In accordance with Floquet's theorem, the field is either evanescent between the front edge of the perturbation and the cutoff, or resonant in the cavity that builds between the back of the perturbation and the cutoff layer. The last case occurs when a zero of the Airy function crosses the back edge of the perturbation. Over the unstable range (5), the phase response is then made of a succession of regular WKB variations followed by a quick 2π variation corresponding to the occurrence of one new Airy zero between the edge and the cutoff.

The case of Gaussian perturbations is found to be described by a similar relation, provided the width w_f is replaced with an effective width w_{eff}.

$$\Delta\varphi_{max} \approx 2\pi \frac{w_f + w_{eff}}{\lambda_x} = -\frac{8}{3} k_0 L \left[\left(\frac{|x_B|}{L} - \frac{1}{2}\frac{\delta n_0}{n_{cr}} + \frac{w_f}{L} \right)^{3/2} - \left(\frac{|x_B|}{L} - \frac{1}{2}\frac{\delta n_0}{n_{cr}} - \frac{w_{eff}}{L} \right)^{3/2} \right] \quad (9)$$

$w_{eff} \approx 2w_f/3$ accounts both for the Gaussian shape of the envelope and for the shift of the resonance position when x_f varies. It depends weakly on δn_0, w_f, k_f and L.

As the amplitude grows, the phase jumps become sharper and sharper, thus for a finite number of measurements (a finite number of values of x_f or of frequencies), these phase jumps cannot be resolved, leading to a continuous increase of the phase response. This is shown in Figure 3.

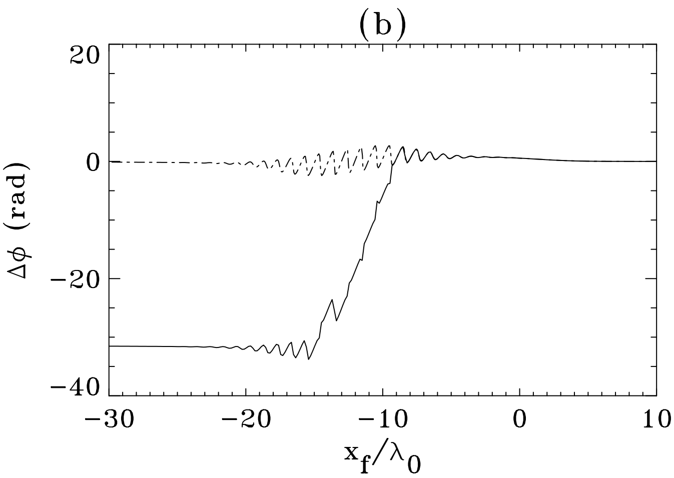

Figure 3. Phase response for a discrete (solid line) or continuous (dashed line) set of Gaussian perturbation positions: $w_f=10\lambda_0$, $k_f=1.2k_0$, $L=400\ \lambda_0$, $\delta n_0/n_{cr}=8\%$

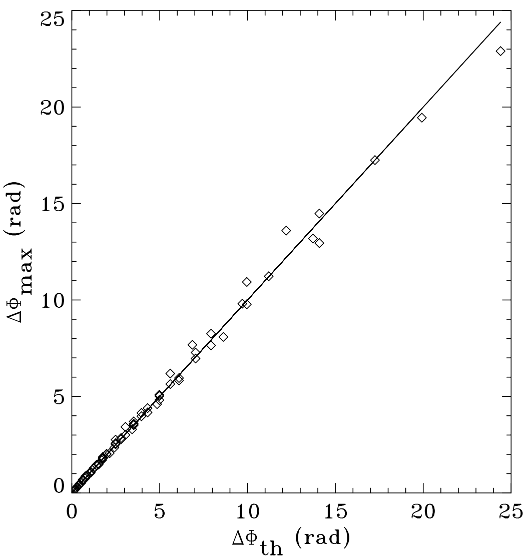

Figure 4. Evolution of the maximum phase shift with the perturbation amplitude. symbols: numerical results; solid line: analytical results

b. Phase response near the cutoff

In that case the phase response exhibits phase jumps similar to that found in the Bragg scattering regime. These phase jumps are related to field resonances occurring in the subcritical cavity which builds up between the unperturbed cutoff layer and the large amplitude perturbation [9]. In the simplest cases, the number of phase jumps and their positions can be analytically estimated. An empirical expression can be found for the maximum phase shift due to Gaussian perturbations

$$\Delta\varphi_{max} = \frac{\sqrt{\pi}}{2} k_0 (w_f L)^{1/2} \left(\frac{k_0}{k_x}\right)^2 \left(\frac{\delta n_0}{n_{cr}}\right)^2 \qquad (10)$$

Figure 4 shows the computed maximum phase shift plotted against the analytical value for more than 100 simulations where L, w_f, k_f and δn_0 are varied. It can be concluded that (10) represents the actual phase variation quite well. In particular, the phase shift scales like the square of the perturbation amplitude, and not linearly, as assumed at small amplitude.

3. Poloidal perturbations: 2D numerical results

We now present numerical results for the 2D Helmholtz equation cases with k_x=0, that is, perturbations with a radial Gaussian envelope and purely azimuthal perturbations. The 2D code is based on a finite difference scheme, with a modified algorithm that guarantees an accuracy in the fourth power of the grid step. The dependence of the signal on the perturbation amplitude, for a perturbation located at the cutoff, has been studied for two different cases: the short wavelength case, λ_y=5 λ_0 and the long wavelength case, λ_y=60 λ_0. One expects that the modulation of the cutoff layer plays a role. Figure 5 shows that the phase evolution is larger for the smallest wavelength. This is in a qualitative agreement with the corrugated mirror model of Conway [3]. However, it is found that the signal amplitude does not vary monotonically, due to interference effects. The effect of a Bragg resonant perturbation (k_y=0.48k_0, x_B=43λ_0) has also been studied. The amplitude evolution is in a qualitative agreement with to the 2D Bragg scattering model of Gusakov [2]. However, in this case the phase does not behave as expected.

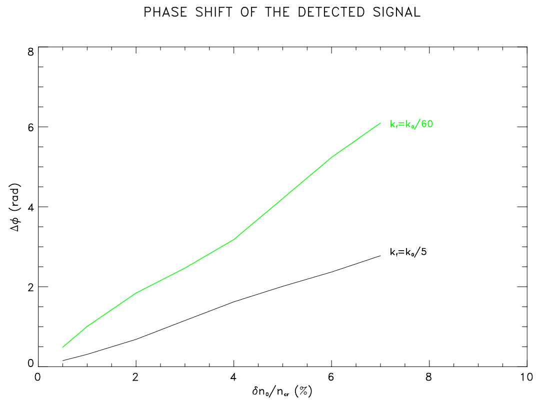

Figure 5. Phase as a function of the perturbation amplitude : λ_y=5λ_0 and λ_y=60λ_0 Perturbation at the cutoff.

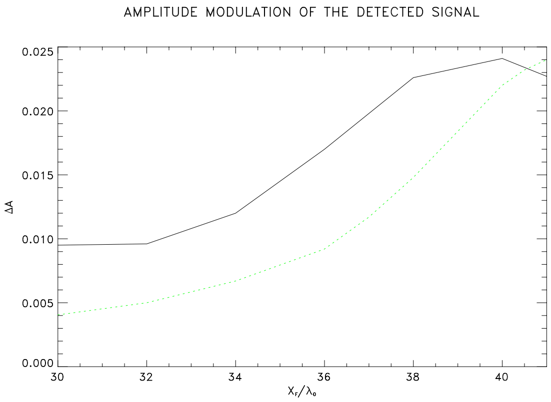

Figure 6. Signal amplitude versus the perturbation position for Bragg resonant perturbation : k_y=0.48k_0, x_B=43λ_0

References

[1] Mazzucato A. 1995 *Rev. Sci. Instrum.* **66** 1237
[2] Gusakov 1996, *Europhys. Conf. Abs*, **V20C, III**, 1136
[3] Conway G. D., Schott L. and Hirose A. 1996 *Rev. Sci. Instrum.* **67** 3861
[4] Conway G. D. 1997 *Plasma Phys. Control. Fusion* **39** 1261
[5] Afeyan B. B., Chou A. E. and Cohen B. I. 1995 *Plasma Phys. Control. Fusion* **37** 315
[6] Fanack C., Boucher I., Clairet F., Heuraux S., Leclert G., Zou X. L. 1996 *Plasma Phys. Control. Fusion* **38** 1915
[7] Chou A. E., Afeyan B. B., and Cohen B. I. 1995 *Rev. Sci. Instrum.* **66** 1216
[8] Abramovitz A. 1976 *Handbook of Mathematical Functions* (New-York : Dover)
[9] Fanack C., Boucher I., Clairet F., Heuraux S., Leclert G., Zou X. L., *Europhys. Conf. Abs*, **V20C, III**, 1148.